Supplementary information

Combustion Co-synthesis of nano SiC and purified Si_3N_4 powders by coupling strong and weak exothermic reactions

Lujia Han,[ab] Huakang Zhang,[ab] Xiao Yang,[a] Yuanyuan Li,[c] Yanhao Dong*[c] and Jiangtao Li*[ab]

[a]*State Key Laboratory of Cryogenic Science and Technology, Technical Institute of Physics and Chemistry, Chinese Academy of Sciences, Beijing 100190, China*

[b]*University of Chinese Academy of Sciences, Beijing 100049, China*

[c]*State Key Laboratory of New Ceramic Materials, School of Materials Science and Engineering, Tsinghua University, Beijing 100084, China*

Table of contents

Supplementary Note 1. Energetic balance calculation: Energy release from Si-N_2 reaction versus energy consumption for Si-C reaction

We calculated the heat required to ignite a unit mass of the Si-C mixture (Q_r). This process involves heating the sample from its initial temperature (T_0, typically ambient temperature at 298 K) to the ignition temperature (T_{ig}) at which a thermal runaway reaction occurs. In our study, we take the melting point of Si (1687 K) as a reasonable and conservative estimate for the ignition temperature.

$$Q_r = C_{p(Si-C)} \times \left(T_{ig} - T_0\right)$$

Where $C_{p(Si\text{-}C)}$ denotes the average specific heat capacity of the Si-C powder mixture.

The average heat capacities ($C_{p,avg}$) between 298 K and 1687 K were calculated by integrating the temperature-dependent polynomial functions for $C_{p(T)}$ provided in the NIST-JANAF Thermochemical Tables.

The calculated values are 907 J kg^{-1} K^{-1} for Si and 1713 J kg^{-1} K^{-1} for graphite：

$$C_{p(Si)} = 907\ J\ kg^{-1}\ K^{-1},\ C_{p(C)} = 1713\ J\ kg^{-1}\ K^{-1}$$

For an Si-C powder mixture in which Si and C are present in a 1:1 molar ratio (corresponding to the stoichiometry of SiC), the mass fractions of Si and C (w_{si} and w_C, respectively) can be expressed as follows:

$$w_{Si} = \frac{n_{Si}M_{Si}}{n_{Si}M_{Si} + n_C M_C} = 0.7\ ,\ w_C = \frac{n_C M_C}{n_{Si}M_{Si} + n_C M_C} = 0.3$$

Where $n_{Si} = n_C$ (i.e., a 1:1 molar ratio), and M_{Si} and M_C denote the molar masses of Si and C, respectively.

$$C_{p(Si\text{-}C)} = w_{Si} \times C_{p(Si)} + w_C \times C_{p(C)} = 1148.8\ J\ kg^{-1}\ K^{-1}$$

$$Q_r = 1148.8 \times (1687 - 298) \approx 1595\ kJ\ kg^{-1}$$

Therefore, heating a unit mass (1 kg) of the Si-C mixture from ambient temperature (approximately 298 K) to the melting point of Si (1687 K) requires approximately 1595 kJ of thermal energy.

Calculation of the heat released per unit mass of the Si-Si_3N_4 mixture upon reaction in N_2 at 3 MPa (Q_s). As an illustrative example, consider silicon powder mixed with 50 wt% Si_3N_4 diluent reacting with nitrogen gas:

$$3Si + 2N_2 \rightarrow Si_3N_4 \quad \Delta H = -736\ kJ\ mol^{-1}$$

The heat released by the reaction of a unit mass (1 kg) of Si with high-pressure N_2 is given by:

$$Q_1 = \frac{\Delta H}{n_{Si} \times M_{Si}} = \frac{736}{3 \times 28} \times 1000 \approx 8762\ kJ\ kg^{-1}$$

Si_3N_4 acts as an inert diluent and does not participate in the chemical reaction. Only the active silicon powder—comprising 50 wt% of the mixture—undergoes reaction and releases heat:

$$Q_s = m_{Si} \times Q_1 = 0.5\ kg \times 8761\ kJ\ kg^{-1} = 4381\ kJ$$

$$Q_s = 2.7 Q_r$$

From this analysis, it follows that even with a high diluent content of 50 wt%, the energy output from the Si-N_2 reaction still amounts to approximately 2.7 times the energy required to ignite the Si-C powder mixture. This indicates that, even under conditions of reduced reactivity, the Si-N_2 system provides sufficient energetic redundancy to initiate and sustain the subsequent Si-C reaction.

Furthermore, considering the significant heat losses that occur in practice, the mass of the Si/Si_3N_4 reaction furnace must exceed the total mass of the Si-C powder mixture used in the experiments to ensure that the combustion synthesis of the Si-C system can be reliably initiated and maintained.

Supplementary Note 2. The stability of the combustion wave propagation during the Si-C reaction process.

It is generally accepted that the unstable effects observed in combustion synthesis processes are fundamentally rooted in thermal dynamics. Specifically, when the reaction enthalpy is insufficient to sustain the stable propagation of the combustion wave, these instabilities emerge.[1] According to the classical stability criterion for combustion wave propagation:[2]

$$\alpha = \left[\frac{9.1}{\left(T_c - T_0\right)} T_c - 2.5 \right] \frac{RT_c}{E} \tag{1}$$

where T_c is the adiabatic combustion temperature (T_c = 1860 K),[3] R is the universal gas constant, 8.314 J mol^{-1} K^{-1}, E is the activation energy (E = 1302.8 kJ mol^{-1}),[4] and T_0 is the initial temperature of the reactant mixture. α = 1 is the boundary separating the stable and unstable combustion modes.

$$\begin{aligned} &\alpha > 1, \quad \text{stable strady state combustion} \\ &\alpha < 1, \quad \text{oscillatory combustion} \end{aligned} \tag{2}$$

When the Si-C reaction mixture was preheated to 1373 K and ignited, the calculated α value was 0.38, indicating unstable combustion wave propagation. Under such conditions, the combustion front exhibited high sensitivity to reaction parameters. Even minor inhomogeneities in the sample or fluctuations in reaction conditions could lead to the extinction of the combustion wave.[5]

Supplementary Note 3. In situ measurement of combustion wave propagation.

The combustion wave front propagation process was in situ monitored using a resistance-displacement response testing system developed by our group.[6] In this work, a constantan resistance wire with a diameter of 0.5 mm was twisted into a 15.4 cm long twisted pair and buried at the center of a Si/C powder mixture (Fig. S13). A constant current was applied to the twisted pair, and the voltage across the resistance wire was measured after the circuit was closed. As the combustion wave front advanced, the length of the twisted pair continuously decreased. Since resistance is linearly related to length, the voltage signal detected by the signal acquisition device continuously varied. Thus, the continuous change in voltage over time represented the continuous change in the length of the resistance wire.

As shown in Fig. S14a, the voltage signal variation is non-uniform, indicating that combustion is non-uniform at the macroscopic level. By converting the voltage signal into combustion wave propagation displacement, Fig. S14b more intuitively reveals that there are distinct hesitation periods during the combustion wave movement. This suggests that the combustion wave front does not propagate at a constant speed but rather stops briefly before continuing to advance, with this cycle repeating. This is consistent with the characteristics of oscillatory combustion.[1]

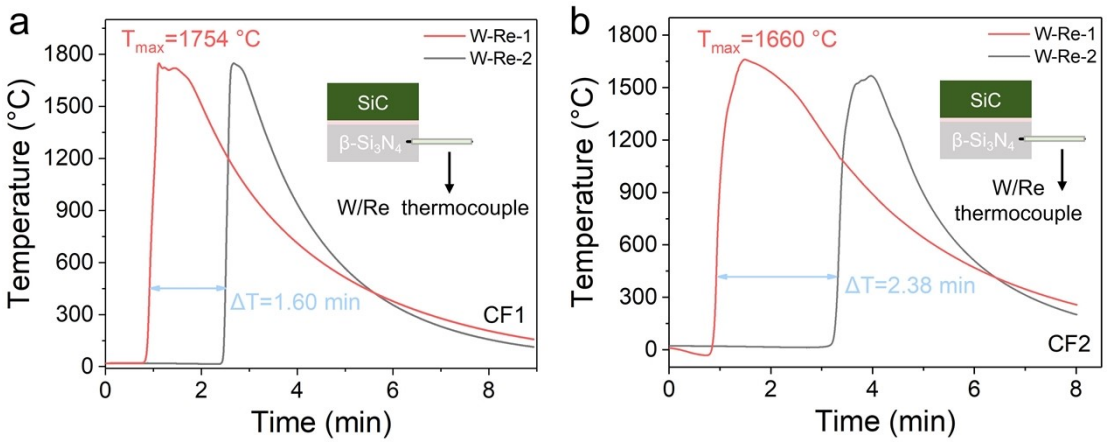

Fig. S1. Characterization of combustion synthesis process in chemical furnace system. (a) Temperature-time curve of the reaction process of the CF1 system; (b) Temperature-time curve of the reaction process of the CF2 system.

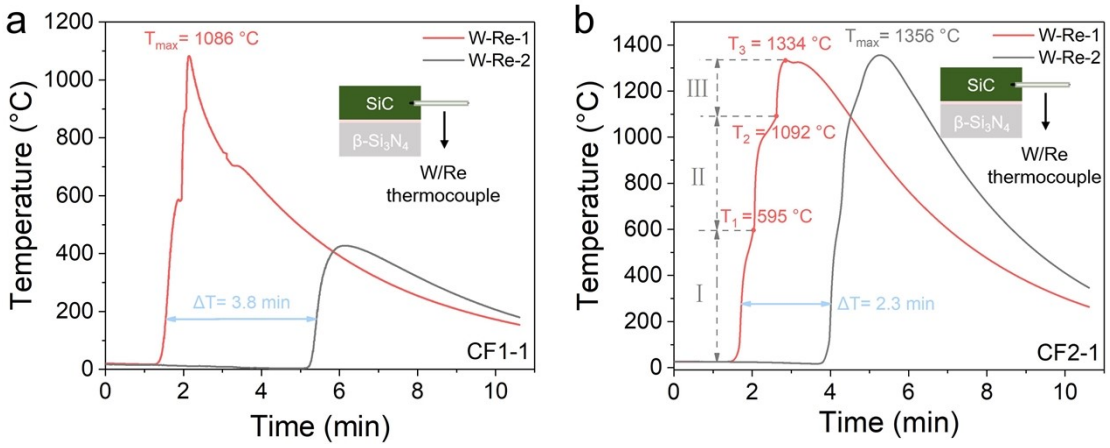

Fig. S2. Temperature-time curves of the Si-C reaction process in different reaction systems. (a) Temperature-time curve of the reaction process of the CF1-1 system; (b) Temperature-time curve of the reaction process of the CF2-1 system.

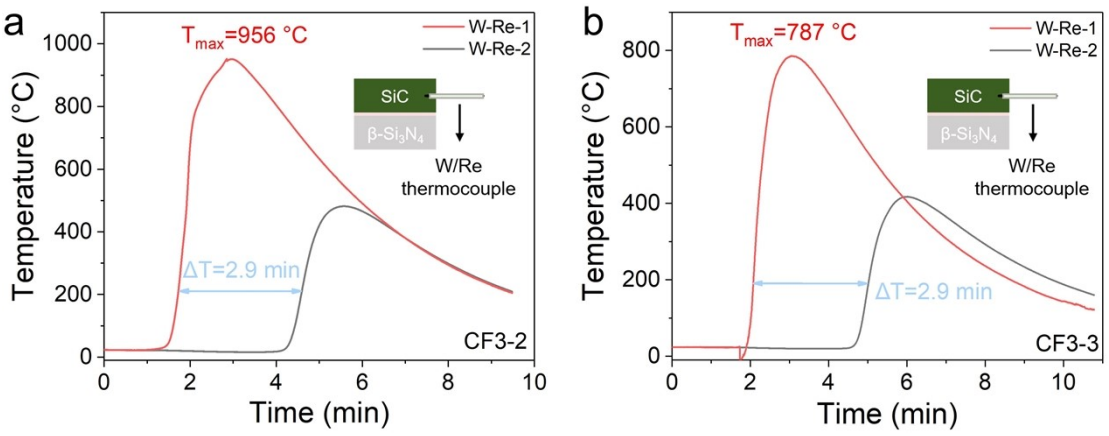

Fig. S3. Temperature-time curves of the Si-C reaction process in different mass ratios of Si-Si_3N_4 and Si/C mixed powder reaction systems. (a) Temperature-time curve of the reaction process of the CF3-2 system; (b) Temperature-time curve of the reaction process of the CF3-3 system.

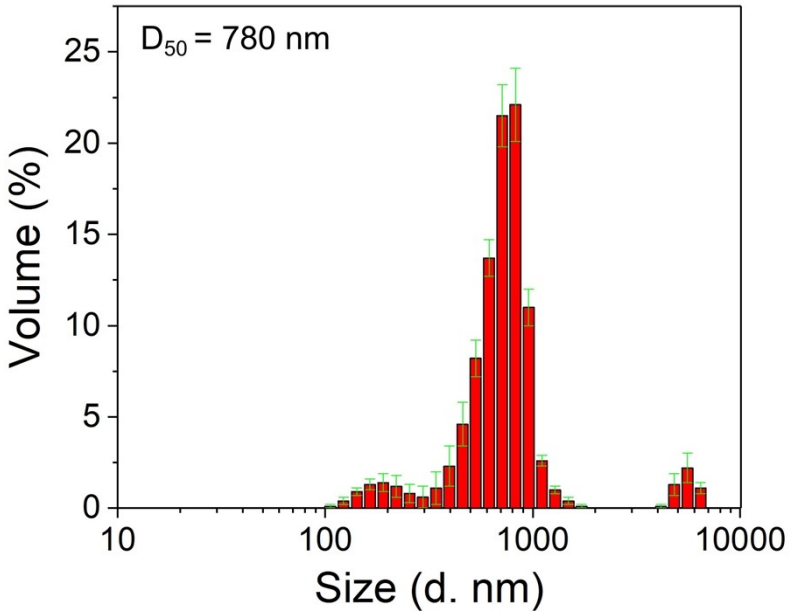

Fig. S4. The particle size distribution of the obtained SiC nanopowder.

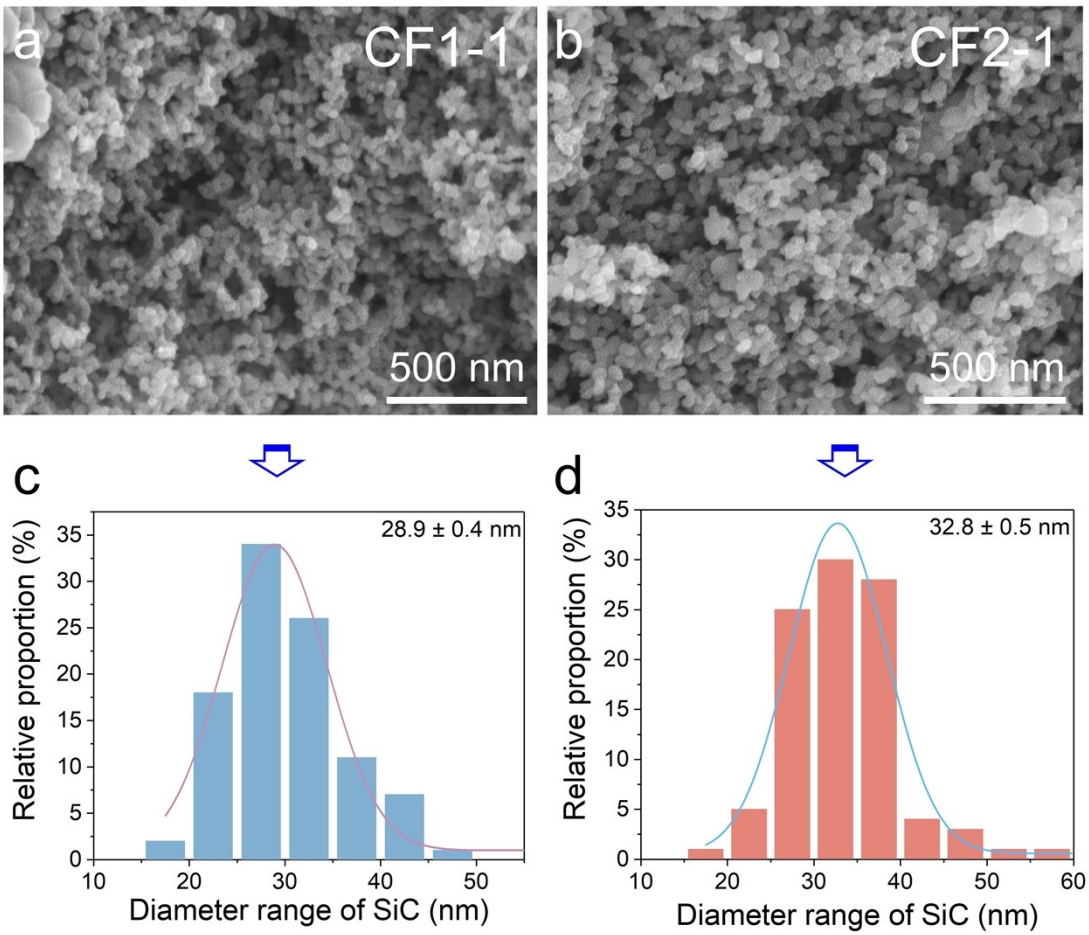

Fig. S5. Microstructure and particle size distribution of SiC nanoparticles. (a) The microstructure and (c) average particle size distribution of SiC particles obtained by CF1-1 reaction system; (b) The microstructure and (d) average particle size distribution of SiC particles obtained by CF2-1 reaction system.

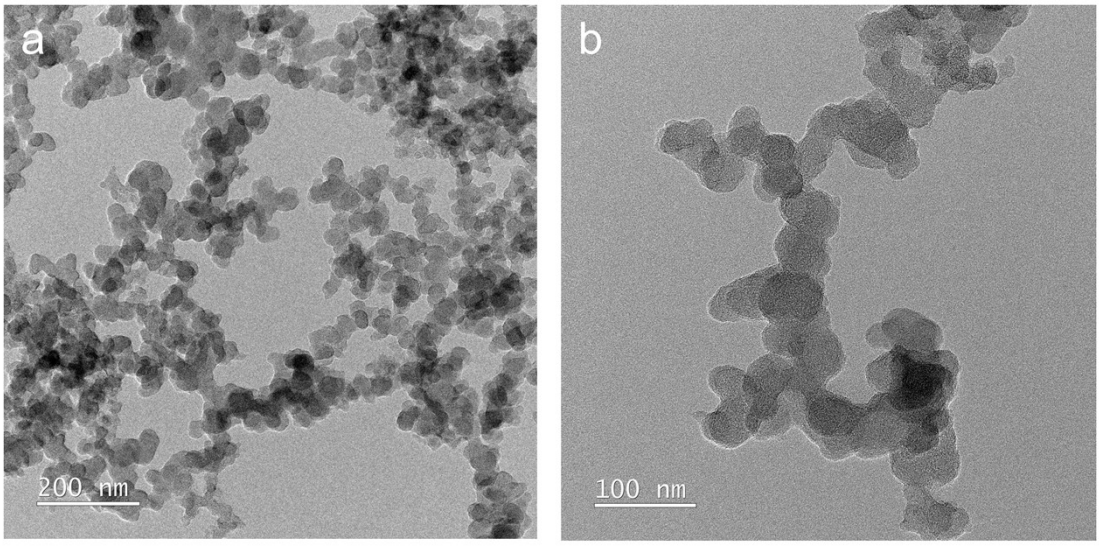

Fig. S6. Microstructure of carbon black raw material. (a) TEM image of carbon black particles; (b) Magnified TEM image of the carbon black particles.

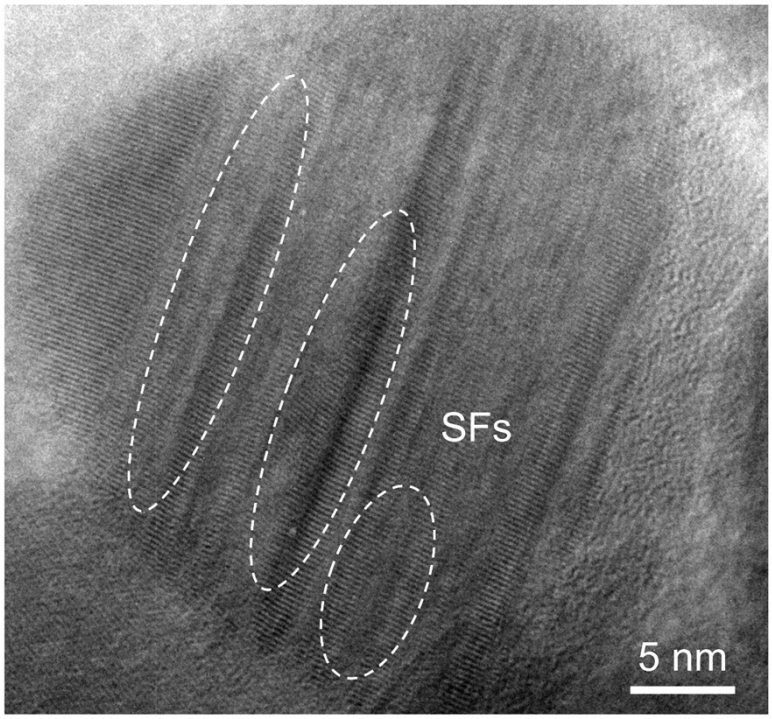

Fig. S7. High-resolution TEM image of SiC nanoparticles.

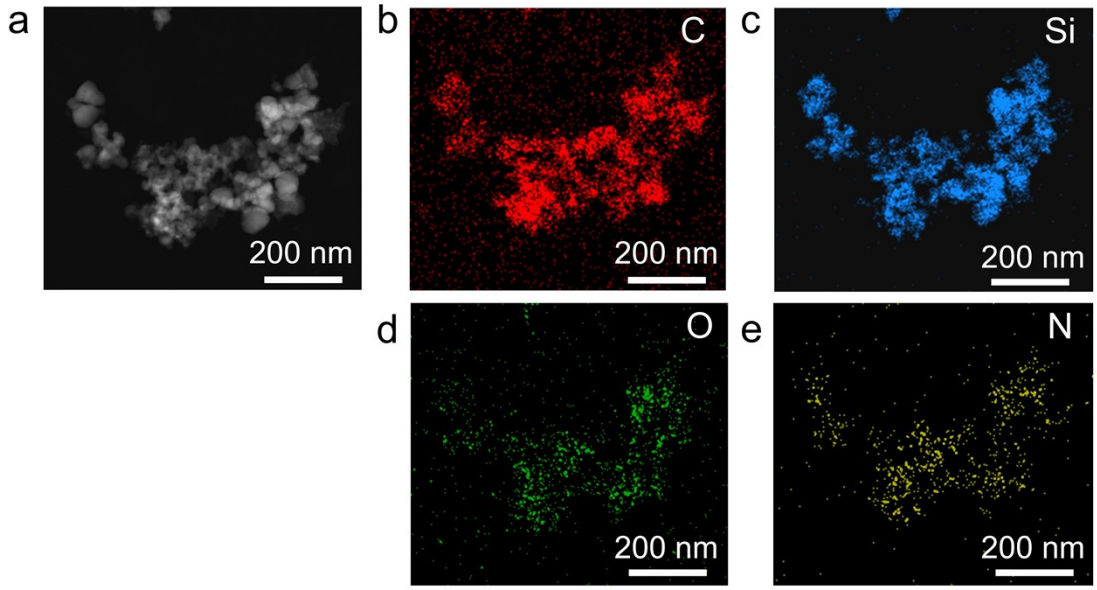

Fig. S8. EDS surface scan analysis of SiC nanoparticles. (a) TEM image of SiC nanoparticles; (b-e) The elemental distribution of C, Si, O and N in SiC nanoparticles.

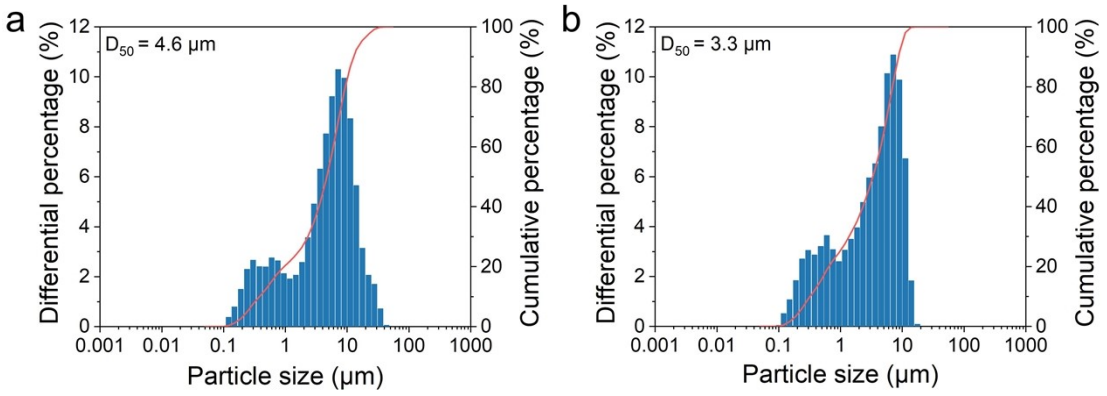

Fig. S9. The particle size distribution of the obtained (a) pink Si_3N_4 and (b) gray-white Si_3N_4 powders.

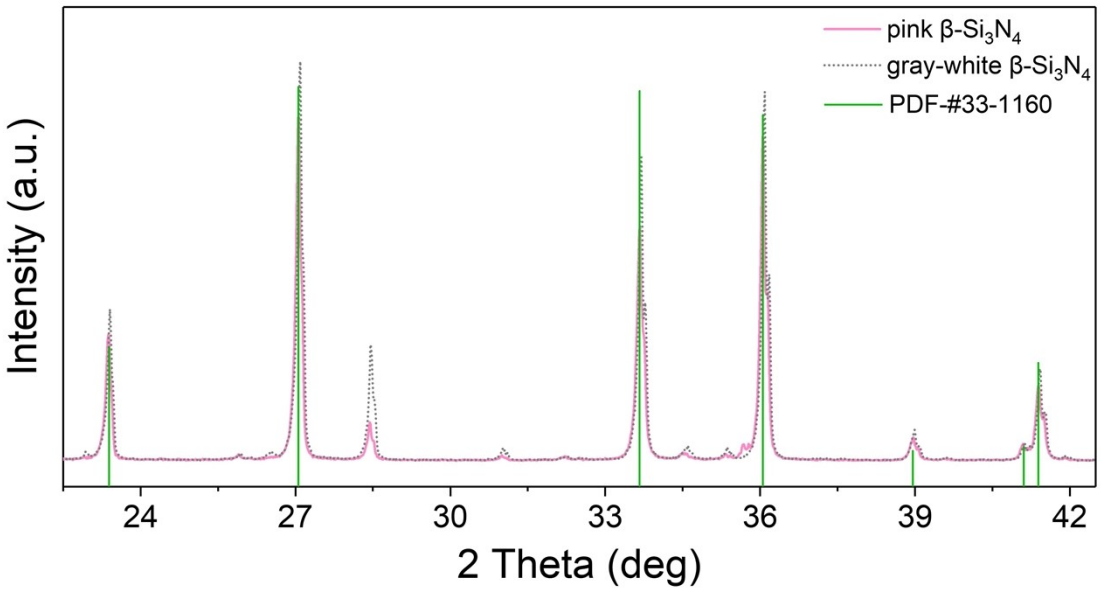

Fig. S10. XRD patterns of pink and gray-white Si_3N_4 powder.

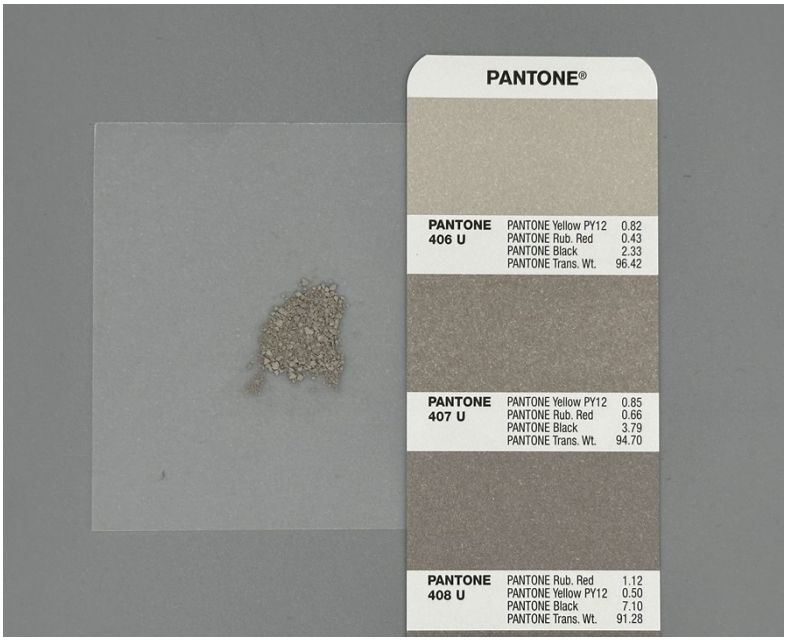

Fig. S11. Optical photograph of pink Si_3N_4 powder after high-temperature treatment (600 ℃, 2 h).

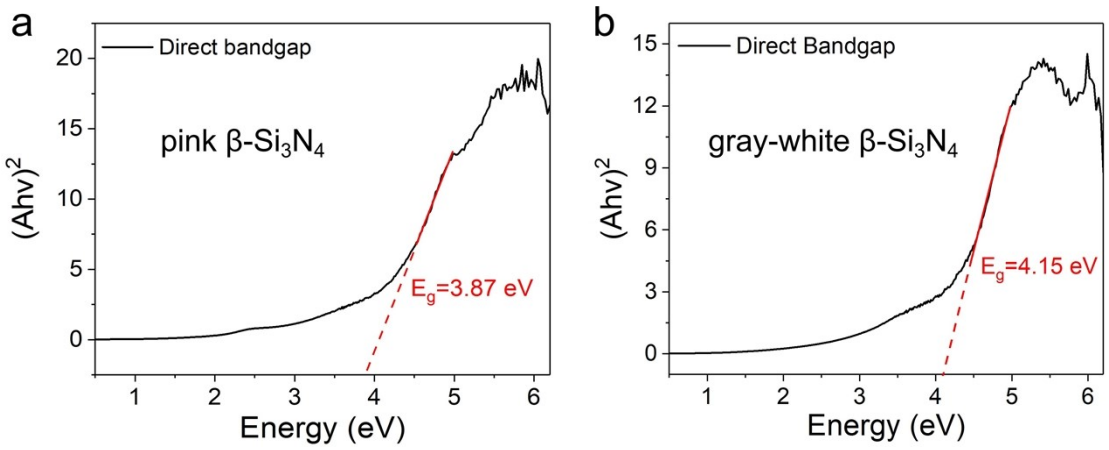

Fig. S12. Direct bandgap calculation of β-Si_3N_4. (a) Direct bandgap calculation of pink β-Si_3N_4; (b) Direct bandgap calculation of gray-white β-Si_3N_4.

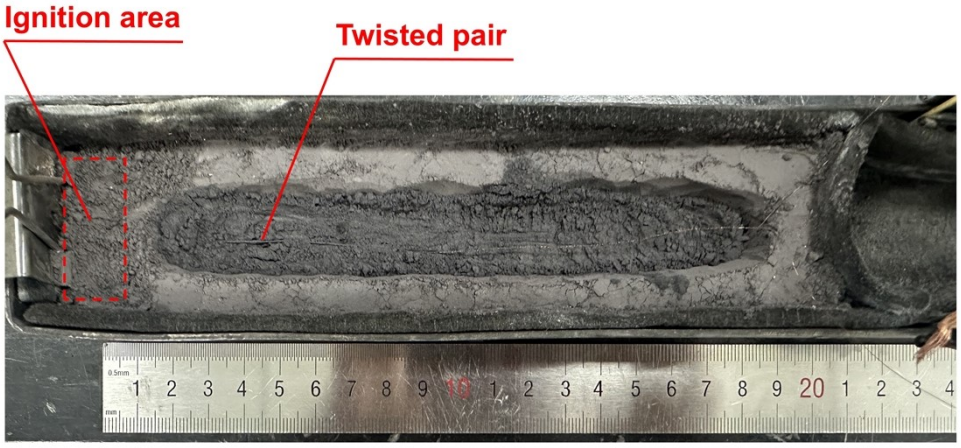

Fig. S13. Optical photo of the placement position of the twisted pair before the reaction (CF3-1).

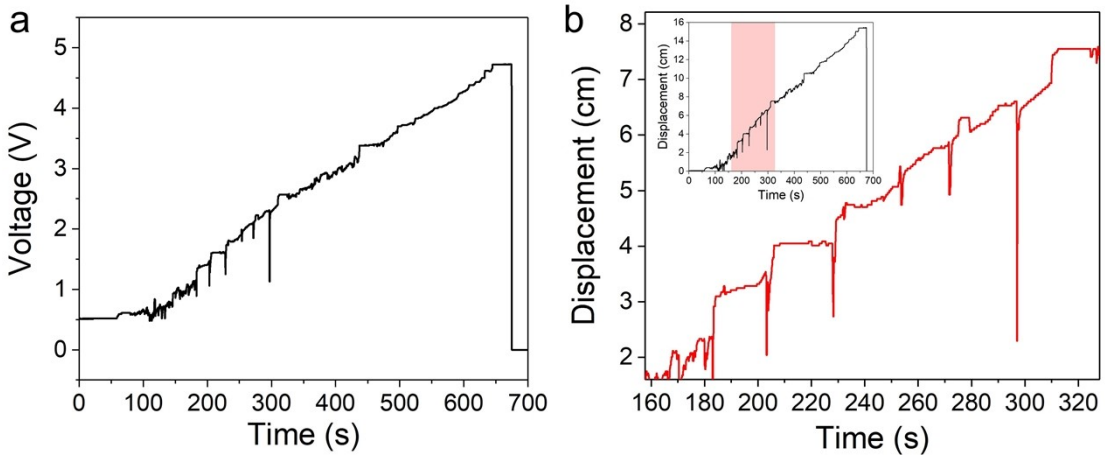

Fig. S14. In situ measurement of combustion wave propagation. (a) Voltage–time curve; (b) Combustion wave displacement–time local amplification curve obtained by combustion synthesis of nano-SiC powder.

Table S1 Propagation velocity of combustion wave and peak reaction temperature of the different Si-N_2 chemical furnace reaction systems.

Chemical furnace reaction ststems	V (mm min^{-1})	T_{max} (℃)
CF1	25.0	1754
CF2	16.8	1660
CF3	17.8	1788

Table S2 Phase composition of Si_3N_4 products obtained from direct Si-N_2 reaction and coupled Si-N_2/Si-C reactions.

Direct Si-N_2 reactions			
Chemical furnaces	β-Si_3N_4 (wt%)	α-Si_3N_4 (wt%)	Residual Si (wt%)
CF1	95.00	4.16	0.84
CF2	92.76	5.36	1.88
CF3	78.95	10.42	10.42
Coupled Si-N_2/Si-C reactions			
Reaction systems	β-Si_3N_4 (wt%)	α-Si_3N_4 (wt%)	Residual Si (wt%)
CF1-1	97.40	2.55	0.06
CF2-1	93.44	6.40	0.16
CF3-1	95.53	2.80	1.66

Table S3 Comparison of different SiC synthesis methods.

Methods	Reaction time	Energy consumption	Particle size	Morphology control	Oxygen content	References
Preheating (SHS)	Seconds to minutes	Medium-High (preheat to 1200 °C)	~130 nm	Moderate, requires grinding	Medium	7
Electric field-assisted (FACS)	Seconds	Low (electric field only)	Up to 25 μm	Low, bulk-like	Medium (contains unreacted Si)	8
Laser CVD	Short (continuous)	High (laser energy)	4-12 nm	Excellent, spherical	High (can be oxidized)	9
Carbothermal reduction	Long (2 h)	Medium (furnace heating)	15–17 nm (crystallite)	Moderate, agglomerated	Medium	10
This work	Seconds to minutes	Low (self-heating)	~30 nm	Good, spherical	Medium (1.5wt%)	/

Table S4 Phase composition of pink Si_3N_4 and gray-white Si_3N_4 products obtained from coupled Si-N_2/Si-C reactions.

Si_3N_4 products	β-Si_3N_4 (wt%)	α-Si_3N_4 (wt%)	Residual Si (wt%)
pink Si_3N_4	96.92	2.50	0.58
gray-white Si_3N_4	95.53	2.80	1.66

Supplementary References

1. A. Mukasyan, A. Rogachev and A. Varma, Mechanisms of pulsating combustion during synthesis of advanced materials, *AIChE J.*, 1999, **45**, 2580–2585.
2. B. Novozhilov, Non-linear SHS phenomena: Experiment, theory, numerical modeling, *Pure Appl. Chem.*, 1992, **64**, 955–964.
3. N. Amirkhanyan, H. Kirakosyan, M. Zakaryan, A. Zurnachyan, M. Rodriguez, L. Abovyan and S. Aydinyan, Sintering of silicon carbide obtained by combustion synthesis, *Ceram. Int.*, 2023, **49**, 26129–26134.
4. H. Wu, S. Huang, H. Qiu, H. Zhu, Z. Xie, Effect of Si and C additions on the reaction mechanism and mechanical properties of FeCrNiCu high entropy alloy, *Sci. Rep.*, 2019, **9**, 16356.
5. G. Liu, K. Yang, J. Li, K. Yang, J. Du and X. Hou, Combustion synthesis of nanosized β-SiC powder on a large scale, *J. Phys. Chem. C*, 2008, **112**, 6285–6292.
6. L. Wang, Z. Yang and J. Li, In situ measurement of combustion wave propagation during combustion synthesis of α-Si_3N_4 powder, *J. Am. Ceram. Soc.*, 2023, **106**, 4023–4027.
7. R. Pampuch, L. Stobierski and J. Lis, Synthesis of sinterable beta-SiC powders by a solid combustion method, *J. Am. Ceram. Soc.*, 1989, **72**, 1434–1435.
8. A. Feng and Z. Munir, The effect of an electric field on self-sustaining combustion synthesis: Part II. Field-assisted synthesis of β-SiC, *Metall. Mater. Trans. B,* 1995, **26B**, 587–593.
9. Y. Kamlag, A. Goossens, I. Colbeck and J. Schoonman, Laser CVD of cubic SiC nanocrystals, *Appl. Surf. Sci.*, 2001, **184**, 118–122.
10. M. Sharma, R. Upadhyay, S. Amritphale and N. Chandra, Synthesis of nano-structured 3C-SiC by carbothermal reduction of silicon bearing gel and carbon soot, *Mater. Lett.*, 2011, **65**, 2161–2164.